FINAL REPORT---UNIV OF CALIF-DAVIS----AWARD NO DE-FG02-04ER15546

Report for the DOE Grant on "Electronic Structure of Transition Metal Clusters, Actinide Complexes and Their Reactivities"

Table of Contents

Introduction

1.1 Collaborations with experimentalists and Theorists

This is a continuing DOE-BES funded project on transition metal and actinide containing species, aimed at the electronic structure and spectroscopy of transition metal and actinide containing species. While a long term connection of these species is to catalysis and environmental management of high-level nuclear wastes, the immediate relevance is directly to other DOE-BES funded experimental projects at DOE-National labs and universities. There are a number of ongoing gas-phase spectroscopic studies of these species at various places, and our computational work has been inspired by these experimental studies and we have also inspired other experimental and theoretical studies. Thus our studies[1-27] have varied from spectroscopy of diatomic transition metal carbides to large complexes containing transition metals, and actinide complexes that are critical to the environment. We have collaborated with experimentalists such as Prof Lester Andrews (U of VA), Prof Heino Nitsche (LBNL and UC Berkeley), Prof John Lombardi (City College, NY), Dr. Patrick Allen (Livermore, EXAFS study), Dr. Annie Kersting (Livermore environmental science) and have also collaborated with theorists such as Prof Henry F. Schaefer III on a baffling problem on AgSiO. We are also in touch with many experimental groups (Professors A. W. Castleman of PSU, Mike A. Duncan of UGA, Dan Neumark at LBNL/UCB, Lai-Sheng Wang of PPNL-WSU, Mike Morse, Bill Weltner at Florida, V. E. Bondybey, Neeb, Dr. John Gibson of ORNL and so on). In addition, we are continuing to make code enhancements and modernization of ALCHEMY II set of codes and its interface with relativistic configuration interaction (RCI). At present these codes can carry out multi-reference computations that included up to ***60 million configurations*** **and multiple states** from each such CI expansion. ALCHEMY II codes have been modernized and converted to a variety of platforms such as Windows XP, and Linux. We have revamped the symbolic CI code to automate the MRSDCI technique so that the references are automatically chosen with a given cutoff from the CASSCF and thus we are doing accurate MRSDCI computations with 10000 or larger reference space of configurations. The RCI code can also handle a large number of reference configurations, which include up to 10,000 reference configurations. **Another major progress is in routinely including larger basis sets up to 5g functions in thee computations**. Of course higher angular momenta functions can also be handled using Gaussian and other codes with other methods such as DFT, MP2, CCSD(T), etc. We have also calibrated **our RECP**

methods with all-electron Douglas-Kroll relativistic methods. We have the capabilities for computing full CI extrapolations including spin-orbit effects and several one-electron properties and electron density maps including spin-orbit effects.

We are continuously collaborating with several experimental groups around the country and at National Labs to carry out computational studies on the DOE-BES funded projects. The past work in the last 3 years was primarily motivated and driven by the concurrent or recent experimental studies on these systems. We were thus significantly benefited by coordinating our computational efforts with experimental studies.

Table I Collaborations with experimentalists at National Labs and Universities

Collaborator	Organization	Nature of Problem/Molecule/System
Prof. Heino Nitsche	LBNL	Expt-Theory Interaction on Uranyl complexes with silicates , carbonates & phosphates
Prof John Lombardi	CUNY	Raman Spectra of transition metal clusters
Prof Michael D. Morse	U OF Utah	Resonance Photon ionization spectra of Transition metal carbides
Drs. Patrick G. Allen & Ann Kersting, Wigbert Sikehaus	LLNL	Environmental-Actinide chemistry & Actinide Surface science
Prof. Henry F. Schaefer	U of GA	Potential Energy Surfaces of AgSiO
Prof Leroy Chauffe	CSU Eastbay	Uranyl complexes
Dr. John K. Gibson	ORNL	IPs of small Actinide molecules

The interaction between theory and experiment has resulted in some unique and exciting opportunities. For example, for the very first time ever, the upper spin-orbit component of a heavy trimer such as Au_3 was experimentally observed as a result of our accurate computational study on the upper electronic states of gold trimer. Likewise for the first time AuH_2 could be observed and interpreted clearly due to our computed potential energy surfaces that revealed the existence of a large barrier to convert the isolated AuH_2 back to Au and H_2.

We have also worked on yet to be observed systems and have made predictions for future experiments. We have computed the spectroscopic and thermodynamic properties of transition metal carbides transition metal clusters and compared our electronic states to the anion photodetachment spectra of Lai Sheng Wang. Prof Mike Morse and coworkers(funded also by DOE-BES) and Prof Stimle and coworkers(also funded by DOE-BES) are working on the

spectroscopic properties of transition metal carbides and nitrides. Our predictions on the excited states of transition metal clusters such as Hf_3, Nb_2^+ etc., have been confirmed experimentally by Prof. Lombardi and coworkers using resonance Raman spectroscopy.

We have also been studying larger complexes critical to the environmental management of high-level nuclear wastes. In collaboration with experimental colleague Prof Hieno Nitsche (Berkeley) and Dr. Pat Allen (Livermore, EXAFS) we have studied the uranyl complexes with silicates and carbonates. It should be stressed that although our computed ionization potential of uranium oxide was in conflict with the existing experimental data at the time, a subsequent gas-phase experimental work by Prof Mike Haven and coworkers published as communication in JACS confirmed our computed result to within 0.1 eV. This provides considerable confidence that the computed results in large basis sets with highly-correlated wave functions have excellent accuracies and they have the capabilities to predict the excited states also with great accuracy. Computations of actinide complexes (Uranyl and plutonyl complexes) are critical to management of high-level nuclear wastes. The geometrical and electronic properties such as ionization potentials, electron affinities, and binding energies of transition metal clusters vary dramatically. These studies are made with relativistic complete active space multi-configuration self-consistent-field (CASSCF) followed by large-scale CI computations and relativistic CI (RCI) computations up to 60 million configurations.

1.2 Educational Outreach in Actinide Chemistry

It has been well recognized that training of young research associates and students in the general area of actinide chemistry is critical to the future of our nation, as there has been a recognized dearth of computational and experimental actinide chemists. Table II demonstrates our vigorous effort s to educate and increase minority students in actinide chemistry.

Table II List of students/research associates who participated in the project.

Name	Degree	Ethnicity/Gender	Participation
Veronica Wheaton	MS	African-American(F)	Uranyl Silicate
Tomekia Simeon	PhD	African-American(F)	Metal-substituted fullerenes&nonowores
Analisa DelVito	PhD	Latino/Female	W clusters + CO
Doyel Chaudhuri	Post-doc	Asian/Female	Plutonyl carbonate
Sanjukta Behera	Research Associate	Asian/Female	Transition-metal complexes
Pablo Denis Marinoni	Research Associate	Hispanic (M)	TM Carbides

2 Electronic structure of metal clusters

2.1Treacherous Potential Energy Surface of AgSiO[6]

The AgSiO system has been a source of puzzlement for more than a decade, with experimental and theoretical studies providing bewildering conclusions regarding the structure of the molecule. State-of-the-art coupled cluster and multireference configuration interaction methods have been applied in collaboration with Professor Henry F. Schaefer (U of GA).[6] We have also incorporated techniques designed to incorporate relativistic effects. With the CCSDCT) method, the Ag-SiO dissociation energy is predicted to be 6.8 kcal/mole, with the equilibrium structure being a nearly isosceles triangle. However, a second minimum an Ag-O-Si structure with bond angle ~150˚lies less than one kcal/mole. With the multireference CI approach (up to 48 million configurations) the energetic order of these two minima is reversed. In contrast both second-order perturbation theory and density functional theory (DFT) predict an Ag-Si-O structure with bond angle ~115˚ to be the global minimum.

Table III Optimized AgSiO geometries, energy differences and vibrational frequencies at MRSDCI level

State	Geometry	R_1(Ag-Si) (Å)	R_2(Si-O) (Å)	R_3(Ag-O) (Å)	ΔE (eV)[a]	
					MRSDCI	MRSDCI+Q
$^2A_1$ ($^2\Sigma$)	Ag-O-Si (a)	4.215	1.522	2.693	-0.153	-0.151
$^2A'$	Ag-O-Si (b)	4.003	1.505	2.623	-0.166	-0.155
$^2A'$	O-Si-Ag (c)	2.964	1.513	2.725	-0.095	-0.147
$^2A_1$ ($^2\Sigma$)	O-Si-Ag (e)	4.842	1.501	6.343	-0.010[c]	-0.025[c]
	Ag (^{2}S) +SiO ($^1\Sigma$)		1.523[b]		0.000	0.000

Fig 1 Different geometries for AgSiO obtained at various theoretical levels. The obtuse structure b and acute structure c are close at the highest MRSDCI+Q and CCSD(T) levels, while the obtuse structure d is lowest at the DFT and MP2 levels

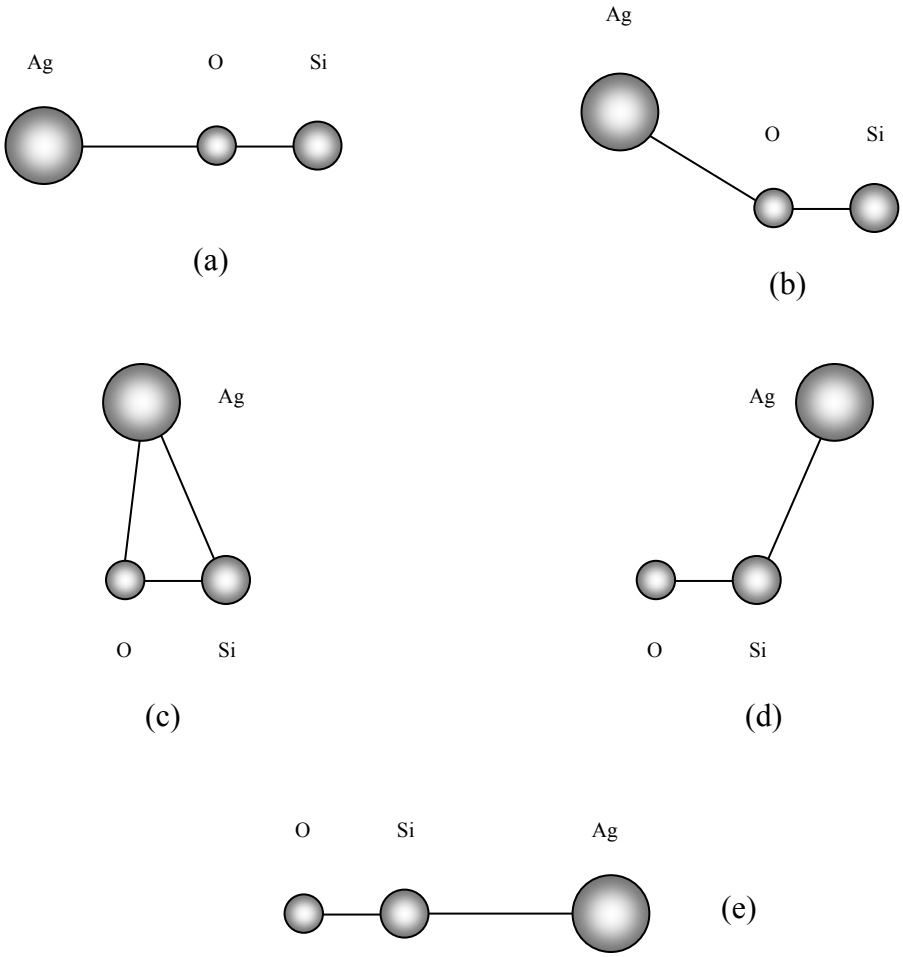

The complex between silver atom and the SiO molecule has been the subject of a number of apparently conflicting experimental and theoretical studies in the last decade. One of the primary motivations for such studies is that the interaction of transition metal species with small molecules is critical to our understanding of chemisorption and surface science. Furthermore there is great interest in studies of the interaction of the transition metal systems with CO, and thus an important question that arises is how similar or different is the SiO molecule in its interaction with transition metals. Finally study of SiO complexes of transition metals can provide critical information pertaining to the energetics of silicon wafer technology. In contrast to the carbonyl complexes of transition metals, there is considerable uncertainty on the structures of SiO complexes of transition metals. In particular the AgSiO complex is quite baffling as it exhibits a number of low-lying structures leading to conflicting predictions. Moreover, there appears to be disarray among the ranks of experimentalists and theorists on the nature of AgSiO up to now.

In view of considerable controversy between experiment and theory, we have studied different geometrical arrangements of AgSiO at very high CASSCF/MRSDCI levels that

included up to 48 million configurations in conjunction with large basis sets that included multiple sets of polarization functions. The results of our computations are shown in Fig 1 and Table III. Both the CCD and MRSDCI results reveal the co-existence of two energy minima, which are very close in energy, one with a bridged triangular structure (c in Fig. 1), and a bent (b in Fig. 1) Ag-OSi structure. The CCSD(T) single point calculations place the bridged triangular structure (c) lower in energy, while the CCD and MRSDCI+Q results favor the bent (b) Ag-OSi structure. The structure (d in Fig. 1) with a bent Ag-SiO arrangement was found to exist only at lower DFT and MP2 levels. The dissociation energy of the AgSiO cluster was found to be 0.16 eV at the MRSDCI+Q level and 0.20 eV at the CCD level for the bent Ag-OSi structure, while CCSD(T) predicts that the bridged triangular geometry has a bonding energy at about 0.29 eV (6.8 kcal/mole). Our theoretical results were used to provide plausible explanations of all previous experimental observations. The calculated asymmetrical vibrational frequency of the AgSiO cluster at the CCD level was found to be in good agreement with experiment.

2.2 Niobium Clusters Computations & Challenges [Trimers-Pentamers][8,13]

Geometries and energy separations of the various low-lying electronic states of Nb_n and Nb_n^- (n = 3, 5) clusters with various structural arrangements were investigated[8,13] due to considerable experimental interest and uncertainty regarding the geometries and low lying electronic states. The complete active space multi-configuration self-consistent field (CASMCSCF) method followed by multi-reference singles and doubles configuration interaction (MRSDCI) calculations that included up to 52 million configuration spin functions have been used to compute several electronic states of these clusters. Details of our computations on Nb_3 can be found in ref. 8. The electronic states of Nb_3 were found to exhibit Jahn-Teller distortion. The ground states of both Nb_4 ($^1A'$, pyramidal) and Nb_4^- ($^2B_{3g}$, rhombus) are low-spin states at the MRSDCI level. The ground state of Nb_5 cluster is a doublet with a distorted trigonal bipyramid (DTB) structure. The anionic cluster of Nb_5 has two competitive ground states with singlet and triplet multiplicities (DTB). The low-lying electronic states of these clusters have been found to be distorted due to *Jahn-Teller* effect. On the basis of the energy separations of our computed electronic states of Nb_4 and Nb_5, we have assigned the observed photoelectron spectrum of Nb_n^- (n = 4, 5) clusters. We have also compared our MRSDCI results with density functional calculations. The electron affinity, ionization potential, dissociation and atomization

energies of Nb_4 and Nb_5 have been calculated and the results have been found to be in excellent agreement with the experiment.

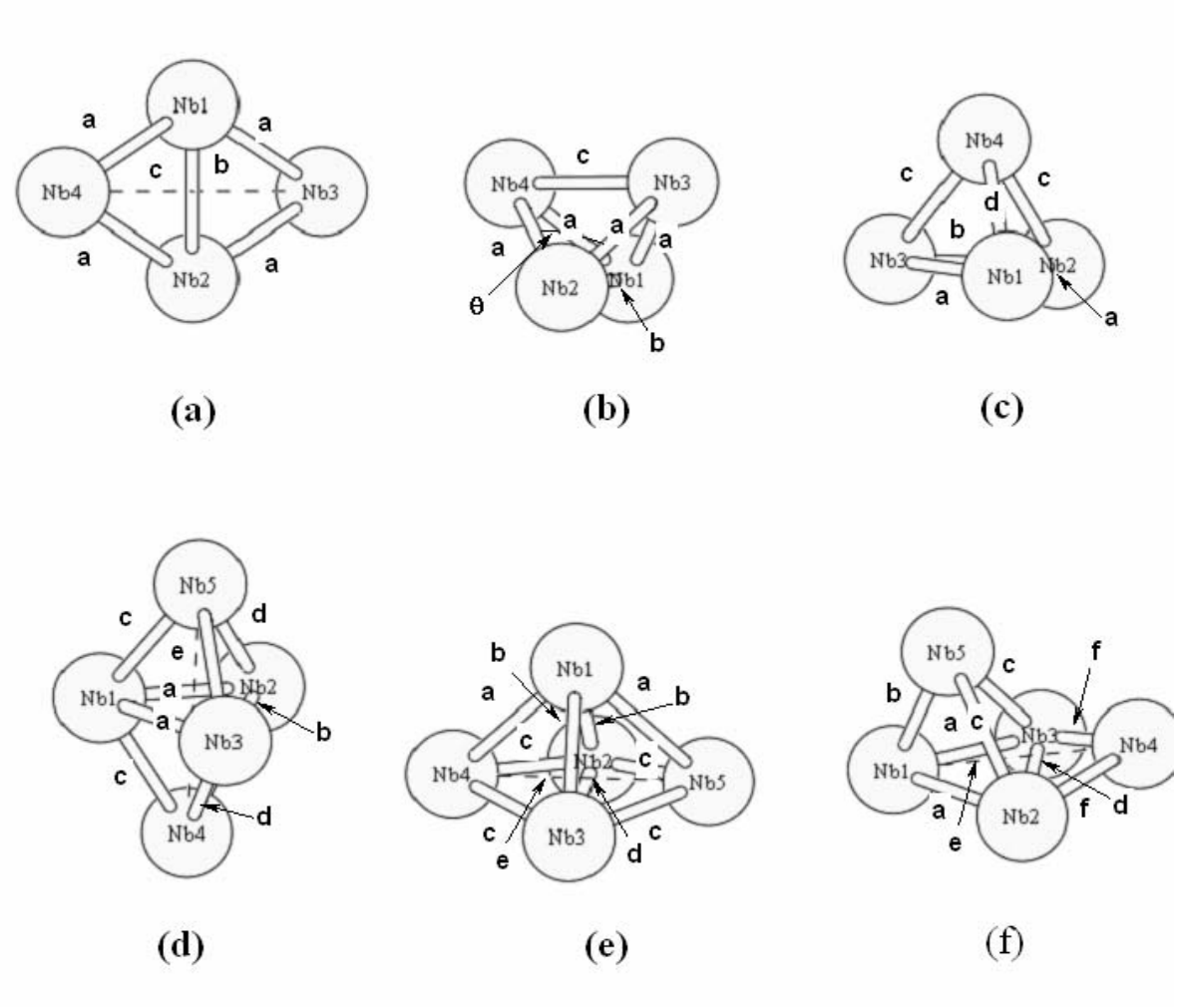

Fig 2 Computed Low –lying Geometries of Nb_4 and Nb_5 Clusters

Fig 2 shows our computed low-lying geometries for the electronic states of Nb_4 and Nb_5 clusters. Tables IV and V show the geometry parameters and energy separations of the neutral and anion species. On the basis of our computed results we assigned the observed spectra of Nb_n^-.

TABLE IV. Bond lengths (a, b, c,…)[a], relative energies (ΔE) of the $^1E'$, $^1A'$, and $^1A''$ states of Nb_4 (at the DFT/B3LYP and MRSDCI levels), and the $^2E''$, $^2A_2$, and $^2B_2$ states of Nb_5 (DFT/B3LYP level).

Cluster	Method	State	a	b	C	d	e	ΔE
			(Å)	(Å)	(Å)	(Å)	(Å)	(eV)
Nb_4	DFT/B3LYP	$^1A'$	2.538	2.538	2.538	2.538		0.00
		$^1A''$	2.497	2.822	2.497	2.551		0.68
		^1E	2.566	2.566	2.566	2.566		2.50
	MRSDCI	$^1A'$	2.713	2.483	2.601	2.568		0.00
	(MRSDCI+Q)							(0.00)

	MRSDCI	$^1A''$	2.614	2.738	2.671	2.616		1.08
	(MRSDCI+Q)							(0.75)
	MRSDCI	$^1E^b$	2.597	2.597	2.597	2.597		1.09[c] (1.14)[d]
	(MRSDCI+Q)							0.78[c] (0.81)[d]
Nb_5	DFT/B3LYP	$^2B_1$	2.644	2.899	2.641	2.512	3.988	0.00
		$^2A_2$	2.836	2.561	2.488	2.576	3.968	0.07
		$^2E''$	2.621	2.621	2.621	2.621	4.279	1.29

[a]Refer to Fig. 1 for the definitions of a, b, c….;[b]geometry optimized at the MRSDCI level.; [c]ΔE calculated from $^1A''$; [d]ΔE calculated from $^1A'$.

Our studies[13] have expounded on the Nb–Nb bonding characteristics and have revealed considerable involvement of both the 5*s* and 4*d* orbitals together with the 5*p* orbital of the Nb atom in the bond. Our study has not only aided understanding of the experimental findings on the PES of Nb_n^- (n = 4, 5), but also predicted properties such as EA, IP and D_e of Nb_n (n = 4, 5), which compare very well with the available experimental data. This gives confidence to our findings on the geometric and electronic properties of the different electronic states of Nb_n and Nb_n^- (n = 4, 5).

We have shown that the ground ($^1A'$, C_s) and the low-lying electronic states of Nb_4 exhibit T⊗e *Jahn-Teller* distortion. We noted that theDFT/B3LYP calculates the *E* state of the T_d structure as a higher root and thus fails to yield proper *Jahn-Teller* description of the electronic states. The ground state of the Nb_5 ($^2A_2$, DTB) cluster has been found to undergo E⊗e *Jahn-Teller* distortion. We have suggested tentative assignments of the observed photo electron spectra of Nb_n^- (n = 4, 5) on the basis of our computed energy separations. The PES of Nb_5^- has three peaks at 1.65, 2.4 (with a shoulder at 2.0 eV) and 3.2 eV.[13] On the basis of the CASMCSCF/MRSDCI ground state of Nb_5 ($^2A_2$, DTB, 1.65 eV peak), the 2.0 eV shoulder peak has been assigned to the $^4A_1$ (DTB) and $^4B_1$ (DTB) states. The intense peak at 2.4 eV has been attributed to the $^4A_1$ (DTP), $^2A_1$ (DTB), and $^6B_2$ (DTB) states. The PES predict the vertical EA of Nb_4 and Nb_5 as 1.15 eV and 1.65 eV respectively. The DFT/B3LYP and MRSDCI results predict

the ground state of Nb_4^- as $^2A'$ (C_s) and $^2B_{3g}$ respectively. According to the CASMCSCF/MRSDCI calculations, the ground state of Nb_5^- has two competitive ground states ($^3B_1$, and $^1A_1$) for the DTB structure. The DFT/ B3LYP level of calculation also suggests two competitive ground states ($^1A_1$, and $^3A_2$, DTB). Our calculated adiabatic EA values based on these ground states of Nb_4^- and Nb_5^- agree with the experimental results very well The computed IP, D_e and the AE of the Nb_4 and Nb_5 are in excellent agreement with the experiment.

TABLE V. Bond lengths (a, b, c…),[a] and energy separations of the electronic states of Nb_4^-

Structure	State	a (Å)	b (Å)	c (Å)	d (Å)	ΔE_{MRSDCI}[b] (eV)	$\Delta E_{MRSDCI+Q}$[b] (eV)
Rhombus (D_{2h})	$^2B_{3g}$	2.318	2.608	3.869		0.00 (0.00)	0.00 (0.00)
	$^4B_{1u}$	2.365	2.705	3.881		0.17 (0.42)	0.23 (0.50)
	$^4B_{2g}$	2.290	2.607	3.767		0.30 (0.28)	0.36 (0.31)
	$^2B_{1u}$	2.356	2.688	3.869		0.76 (0.62)	0.81 (0.72)
	^4A_u	2.324	2.682	3.795		0.62 (1.02)	0.73 (1.12)
	$^2B_{1g}$	2.383	2.651	3.960		1.02 (1.14)	1.07 (1.19)
	$^2B_{3u}$	2.452	2.941	3.926		1.31 (1.85)	1.34 (1.77)
Pyramid (C_s)	$^2A''$	2.403	3.086	3.204	2.430	0.49 (1.57)	0.84 (2.02)
	$^2A'$	2.418	3.228	3.138	2.401	0.49 (1.60)	0.86 (2.09)
	$^4A'$	2.422	3.241	3.241	2.422	0.77 (1.82)	1.19 (2.33)
	$^4A''$	2.381	3.249	3.095	2.517	1.47 (2.50)	1.87 (3.03)

[a]Refer to Fig. 1 for the definition of the bond lengths (a, b, c…) of different structures.
[b]The ΔE values within parentheses are calculated using (5*s*5*p*4*d*1*f*//5*s*3*p*2*d*1*f*) basis set while the ΔE values without parentheses were calculated using (5*s*5*p*4*d*//5*s*3*p*2*d*) basis set of Nb.

2.3 Ruthenium Trimer: Ru_3 (Electronic States and Assignments of observed Spectra)[1]

Several low-lying electronic states of the ruthenium trimer (Ru_3) were investigated by CASSCF and MRSDCI methods that included up to 45 million configurations.[1] Two nearly degenerate states, namely, $^{11}B_1$ and $^{11}B_2$ states were found as candidates for the ground state at

lower level of theory. At the highest MRSDCI level, the $^{11}B_1$ state was found to be the ground state of Ru_3. The atomization energy of this state was further determined with extensive large-scale MRSDCI calculations. Our calculations facilitated assignment of the observed resonance Raman spectra of Ru_3 in Ar matrix by Lombardi and coworkers.

The optimized geometries and energy separations were determined. Most of the electronic states were found to be multiconfigurational in nature, implying the necessity of high-level MCSCF and MRSDCI calculations. The ground state of Ru_3 was found to be $^{11}B_1$ at the highest MRSDCI level. The optimized geometry of this state is as isosceles triangle with Ru-Ru equal distances of 2.673 Å and an apex angle of 94.3º. The vibrational frequencies and atomization energy were reported. The Atomization and dissociation energies of the ground state of Ru_3 were determined with extensive large-scale MRSDCI+Q calculations as 4.44 and 6.16 eV, respectively. Detailed analysis of gross Mulliken populations reveals that the bonding mainly comes from s-p σ donation and p-d π back-donation for states with multiplicity = 11. The 5p orbitals of the ruthenium atom were also found to play an important role in these states. On the basis of our computed energy separations and vibrational frequencies, we have assigned two of the lines in the resonance Raman spectrum of Lombardi and coworkers at 303.4 cm^{-1} and 603.7 cm^{-1} to the fundamental symmetric stretch and overtone of the $^{11}B_1$ ground state. The third Raman line at 581.5 cm^{-1} was attributed to a low-lying excited state of Ru_3, either $^{11}B_2$ or $^{11}A_2$.

3.1 AuH_2—A joint expt-theory study

In collaboration with Prof Lester Andrews, we carried out a joint experimental-theory study on the AuH_2 molecule.[10] Although gold is noble, excited gold is reactive. In spite of this AuH is the most stable of Group 11 monohydrides due to relativistic effects. The AuH_2 molecule was formed in solid hydrogen by reactions of excited gold atoms from laser ablation and irradiation after thermal evaporation. Our computations revealed that the X^2B_2 ground state of the AuH_2 molecule is separated by a 53 kcal/mol barrier from the $Au(^2D) + H_2$ decomposition products and it is 27 kcal/mole more stable than $Au(^2D) + H_2$. The bending modes of AuH_2, AuHD, and AuD_2 have been observed at 638.1, 570.6, and 457.0 cm^{-1}. These frequencies and the lack of infrared intensity in the stretching modes are in agreement with the results of relativistic ECP DFT, MP2 and CCD calculations. The computed bending potential energy surfaces of three electronic states of AuH2 using CASSCF/MRSDCI methods reveal that there is

a barrier for conversion of the X^2B_2 ground state to Au(^{2}S) + H_2. Fig 3 shows the infrared spectra in the 660-420 cm^{-1} region for laser-ablated Au co-deposited with pure hydrogen.

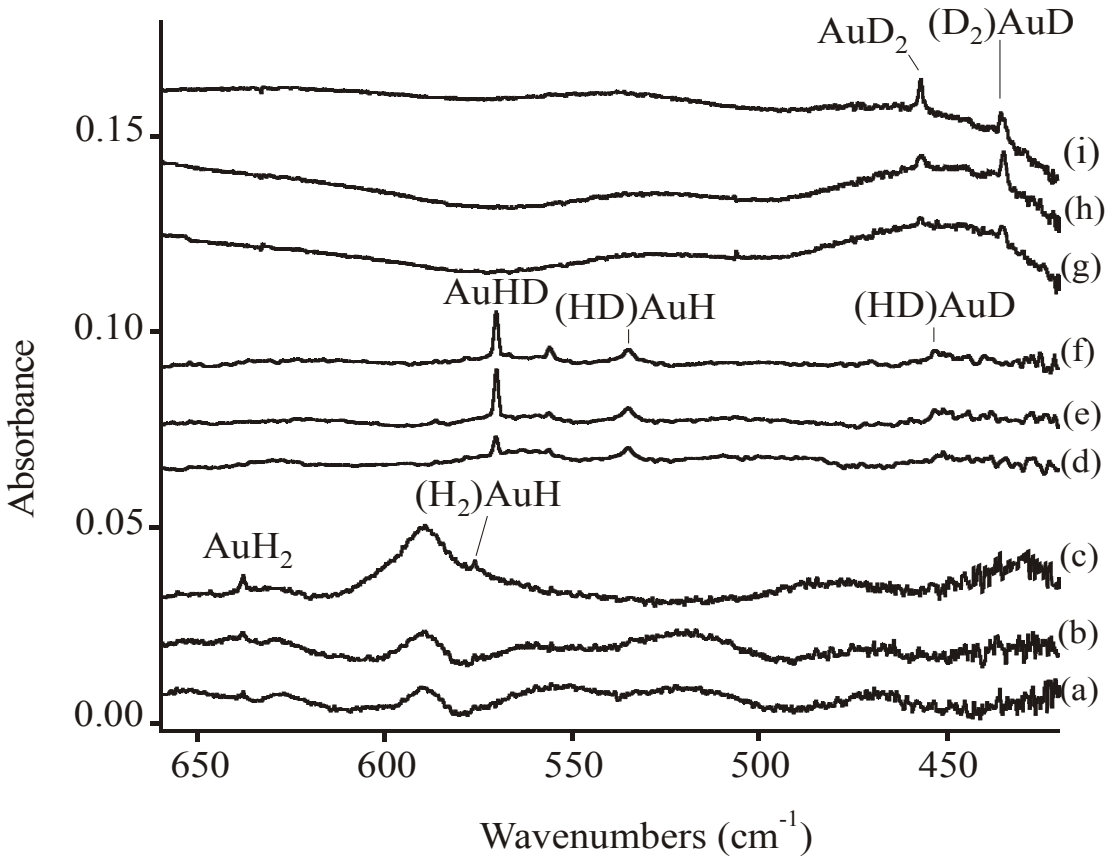

Figure 3. Infrared spectra in the 660-420 cm^{-1} region for laser-ablated Au co-deposited with pure hydrogen isotopic samples at 3.5 K for 25 min. (a) Au + H_2, (b) after $\lambda > 240$ nm photolysis, (c) after annealing to 6.4 K, (d) Au + HD, (e) after $\lambda > 240$ nm photolysis, (f) after annealing to 7.5 K, (g) Au + D_2, (h) after $\lambda > 240$ nm photolysis, and (i) after annealing to 9.0 K.

As seen from Fig 3, the bending modes of AuH_2, AuHD, and AuD_2 have been observed at 638.1, 570.6, and 457.0 cm^{-1}. These frequencies and the lack of infrared intensity in the stretching modes are in agreement with the results of relativistic calculations. We find that the X^2B_2 state of AuH_2 has a stability of 27 kcal/mole relative to Au(^{2}D) + H_2 and is expected to be long-lived in this state due to a large barrier to dissociation. Unlike the X^2B_2 state of AgH_2 which dissociates into Ag(^{2}P) + H_2, the corresponding state of AuH_2 dissociates into Au(^{2}D) + H_2. This is a consequence of the fact that the first excited state of Au atom is ^{2}D, while it is ^{2}P for silver, which is attributed to relativistic stabilization of the 6s orbital of Au and destabilization of the 5d orbital. Figure 4 shows our computed electron density contour plots of the ground state of AuH_2. The plot reveals significant depletion of electronic charge density at the gold site. This is

followed by back donation of electronic charge from the Au(5d π) orbital back into the $1\sigma_u$ antibonding orbital of H_2. The dissociation in the excited state is assisted by the dative mechanism of electron transfer from the gold atom to the hydrogens and back transfer from the H_2 $1\sigma_u$ to Au (d π) and (p π).

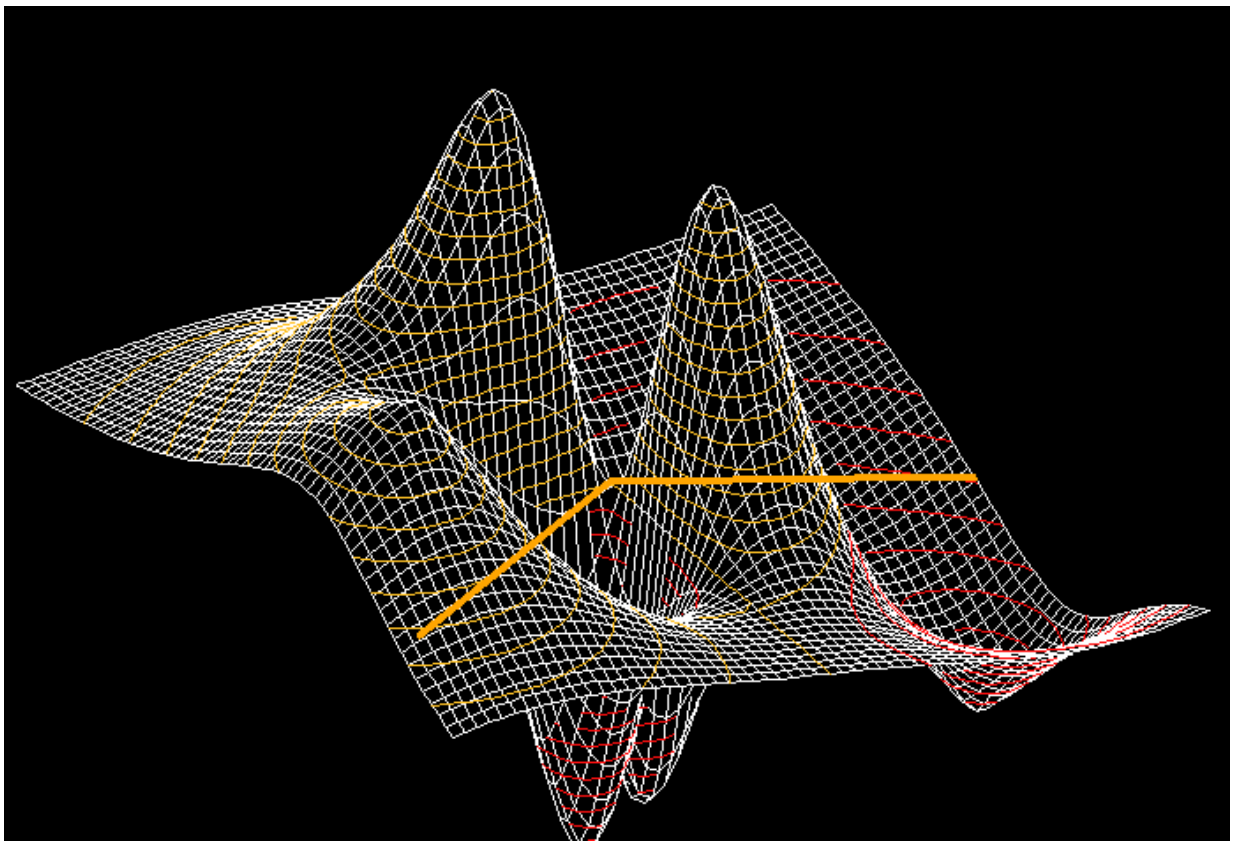

Figure 4 Electron density contour plots of AuH_2 ground state near its minimum geometry. The plot is consistent with a dative electron transfer mechanism of dissociation, where Au sheds electronic charge to the hydrogens and there is back transfer from H_2 $1\sigma_u$ orbital to the Au(5d π).

3.2 Potential Energy Surfaces for Actinide-hydrides: Role of 5f Vs 6d Vs 7p orbitals.[7]

Interaction of actinides with hydrogen through H-H bond activation is of great fundamental and experimental interest as relativity and the nature of 5f and 6d orbitals participation in the H-H bond activation as well as C-H bond activation in hydrocarbons are important to understand. In collaboration with surface science experimentalist at Lawrence Livermore Lab, we have carried out studies on hydrogen activation by actinides such as U and Pu. We have also found surprisingly that Pu forms

hydrides only up to PuH_3 and any further addition of hydrogen results in loose complexes such as $H_2Pu…H_2$ and so on. Likewise our relativistic Lapalcian charge density models have provided significant new insight into the H-H activation by uranium and plutonium.

Fig 5 shows the Laplacians of charge densities of UH_3. The high peaks at the uranium site reveal significant depletion of charge density at the site thus catalyzing further H-H activation, a finding confirmed experimentally.

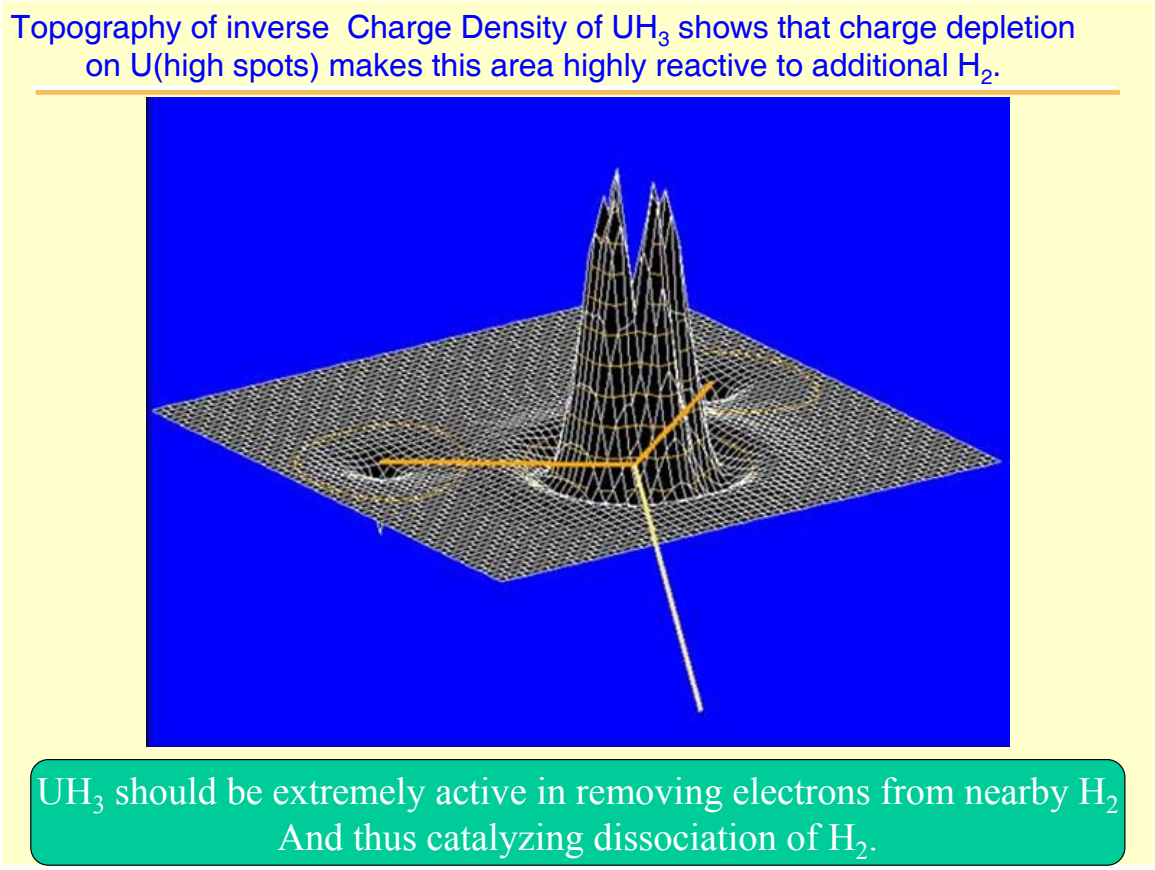

Fig 5 Relativistic Laplacians of charge densities of UH_3

Fig 6 shows our computed equilibrium geometry of PuH_4 and the corresponding IR spectra. It is interesting that even though we stared with a tetrahedral PuH_4 geometry, the lowest structure optimized was that of a complex of $PuH_2..H_2$. This is due to the fact that once the 6d(s) and 6d(p) orbitals are used by two hydrogens in PuH_2 resulting in strong depletion of charge on Pu the additional H_2 forms a weak complex as shown in Fig 6.

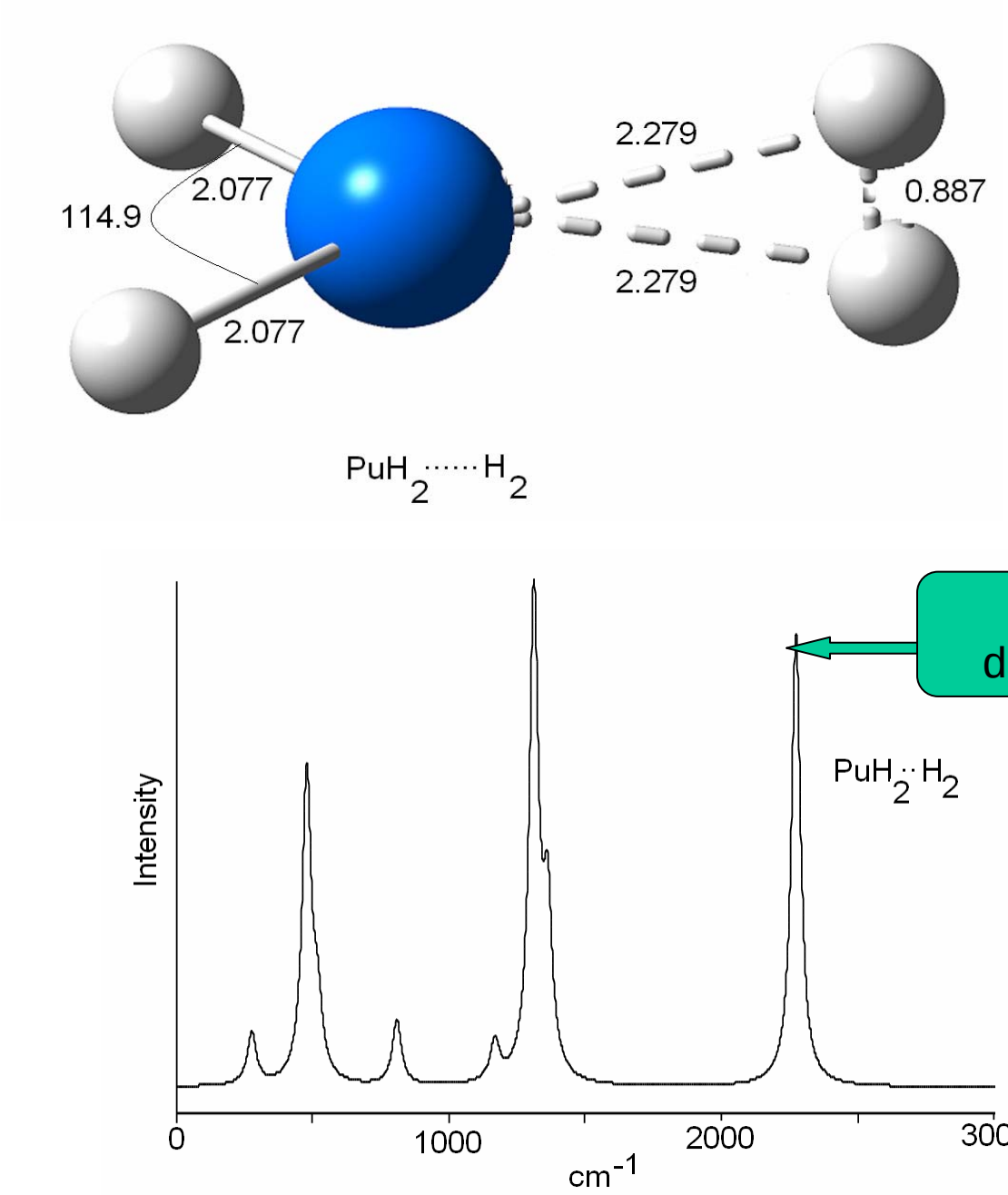

Fig. 6 Optimized structure & Computed IR spectra of $PuH_2…H_2$.

4. *Transition metal carbides*

The transition metal carbides were studied due to their importance in catalysis and compelling need to understand their electronic states and spectra. The optical electronic spectra of these are being actively investigated by DOE-BES funded experimentalists such as Profs. Morse, Steimle, Lai-Sheng Wang and Castleman. Our recent studies included ruthenium carbide, niobium carbide, zirconium and molybdenum carbides . The RuC molecule has been a challenging species

due to the open-shell nature of Ru resulting in a number of low-lying electronic states for this molecule. We have carried out state-of-the-art complete active space multi-configuration self-consistent field followed by multireference configuration interaction methods that included up 18 million configurations, in conjunction with relativistic effects. We have computed 29 low-lying electronic states of RuC with different spin multiplicities and spatial symmetries with energy separations less than 38 000 cm^{-1}. We find two very closely lying electronic states for RuC, viz., $^1\Sigma^+$ and $^3\Delta$ with the $^1\Sigma^+$ being stabilized at higher levels of theory. Our computed spectroscopic constants and dipole moments are in good agreement with experiment although we have reported more electronic states than those that have been observed experimentally. Our computations reveal a strongly bound $X^1\Sigma^+$ state with a large dipole moment and an energetically close $^3\Delta$ state with a smaller dipole moment. Overall our computed energy separations of the excited states with energy separations less than 18000 cm^{-1} agree quite well with experiment.

All of the second-row transition metal carbides are challenging due to the open-shell nature of the metal resulting in a number of low-lying electronic states for this molecule. We have carried out state-of-the-art complete active space multi-configuration self-consistent field followed by multireference configuration interaction methods in conjunction with relativistic effects. For MoC our computed transition energies to the $1^3\Delta$ and $4^1\Delta$ states are 3430 and 8048 cm^{-1} respectively, in fair agreement with the results obtained by Morse and coworkers [JCP 114, 2938, (2001)] namely, 4003 and 7834 cm^{-1} respectively. The three band systems located at 18611, 20700 and 22520 cm^{-1}, observed by Morse et al. [JCP 109, 7851,(1998)] were attributed to the excited $11^3\Sigma^-$, $14^3\Pi$, and $15^1\Pi$ states of MoC. Table VI summarizes dipole moment trends. The 9σ orbital which is predominantly 4s and 5s, points away from the negatively charged carbon, thus occupying this orbital reduces the dipole moment.

Table VI Dipole Moments of Some Second and Third row Transition Metal carbides.

TiC $8\sigma^1 9\sigma^1$, $^3\Sigma^-$ 2.51 Debye	VC $8\sigma^2 1\delta^1$, $^2\Delta$ 7.33 Debye	CrC $8\sigma^2 1\delta^2$, $^3\Sigma^-$ 6.8 Debye	MnC	FeC $8\sigma^2 1\delta^3 9\sigma^1$, $^3\Delta$ 2.36 Debye
ZrC $8\sigma^1 9\sigma^1$, $^3\Sigma^-$ 3.23 Debye	NbC $8\sigma^2 1\delta^1$, $^2\Delta$ 6.77 Debye	MoC $8\sigma^2 1\delta^2$, $^3\Sigma^-$ 5.87 Debye	TcC	RuC $8\sigma^2 1\delta^4$ $^1\Sigma^+$ 4.551 Debye

We have determined that the ground state of ZrC as $^3\sum^+$ although there are two low-lying $^1\sum^+$ states (below 5000 cm^{-1}) which strongly interact resulting in avoided crossings. The lowest $^1\sum^+$ state corresponds to a combination of $1\sigma^2 x\sigma^2 1\pi^4$ configurations whereas the second is an open shell singlet $1\sigma^2 2\sigma^1 3\sigma^1 1\pi^4$. Several avoided crossings were observed, for $^1\Pi$, $^3\Pi$, $^1\Delta$, $^3\sum^+$, and $^3\Delta$ states. We have identified $^3\Pi$ and $^1\Pi$ lying at 4367 and 5797 cm^{-1} respectively. The results are in good agreement with experimental findings of Rixon, Chowdhury and Merer [J. Mol. Spectrosc. 228, 554, (2004)], and indicate that the $^3\Pi$-$^3\sum^+$, and $^1\Pi$-$^1\sum^+$, bands located between 16000-19000 cm^{-1} are extremely complex due to near degeneracy of several $^1\Pi$ and $^3\Pi$.

We have studied the potential energy curves and spectroscopic constants of the ground and low-lying excited states of NbC the complete active space multi-configuration self-consistent field (CASSCF) followed by multireference configuration interaction (MRCI) methods, in conjunction with relativistic effects and 5s3p3d1f, 3s3p1d basis sets con Nb and C respectively. We have identified 26 low-lying electronic states of NbC with different spin multiplicities and spatial symmetries within 40000cm^{-1}. At the MRSDCI level of theory the $^2\sum^+$ and $^2\Delta$ states are nearly degenerated, with the $^2\Delta$ 172 cm^{-1} lower than the $^2\sum^+$ state. However after spin-orbit splitting the $^2\Delta$ state becomes lower by 646 cm^{-1}, in reasonable agreement with the experimental result 831 $cm^{-1.}$ Our computed spectroscopic constants and dipole moments are in good agreement with experiment. On the other hand our results for the excited sates of NbC are different from previous density functional calculation, mainly due to the strong multiconfigurational character of NbC that cannot be handled properly at this level of theory. We have reported more electronic states than those that have been observed experimentally. Our computed results are provided in Table VII for select low lying states of MoC compared to experiment.

TABLE VII. Comparison between experiment and theory for the states of MoC observed in the experimental work.

States	Source	$T_e(cm^{-1})$	r_e (Å)	$\omega_e(cm^{-1})$
$X^3\Sigma^-$	This work	0.0	1.713	974
	Exp. Morse	0.0	1.6877[b]	
	Exp. Lai-Shen Wang	0.0		
$1\ ^3\Delta$	This work	3660	1.711	998

	Exp. Morse	4002.5		1003
	Exp. L. S. Wang	4120		
$2\ ^5\Sigma^-$	This work	5676	1.779	873
	Exp. Li et al	6290		
$3\ ^1\Gamma$	This work	7647	1.693	1030
	Exp. Li et al	5150		
$4\ ^1\Delta$	This work	8198	1.697	1036
	Exp. L. S. Wang	7150		[890(60)]

5. *Actinide Complexes* ……

Our computational studies on actinide complexes were motivated by ongoing EXAFS studies of speciated complexes in geo and biochemical environments carried out by Prof Heino Nitsche's group at Berkeley, Dr. David Clark at Los Alamos and Dr. Gibson's work on small actinide molecules at ORNL. An important driving force behind such studies of actinide complexes is that these are critical to the management of high level nuclear wastes. Actinyl ions in these wastes bind to silicates, carbonates, phosphates and migrate. Thus it is important to understand such actinyl complexes that occur in bio and geochemical environments. We have computed the geometrical and electronic properties as well as vibrational spectra of actinide complexes of environmental importance. These complexes are notoriously difficult and challenging for theoretical studies due to the difficult nature of both 5f and 6d shells and large relativistic and electron correlation effects.

5.1Computational Study of Uranium Carbonates: Unusual predictions…….

We carried out extensive ab initio calculations on the structure and bonding characteristics of $UO_2(CO_3)_2^{2-}$ and $M_2UO_2(CO_3)_2$ (M= Li^+, and Na^+) both in the gas phase and in aqueous solution using coupled cluster doubles (CCD) methods.. The calculated structure and vibrational spectra have been compared with the available experimental data. The nature of the boding in these species is discussed. The presence of such metallic salts is well established experimentally in solution. These biscarbonato metal salts in the solid state form trimers of the type $[M_6(UO_2)_3(CO_3)_6$. These trimetallic clusters can be formed in solution when the metal ion

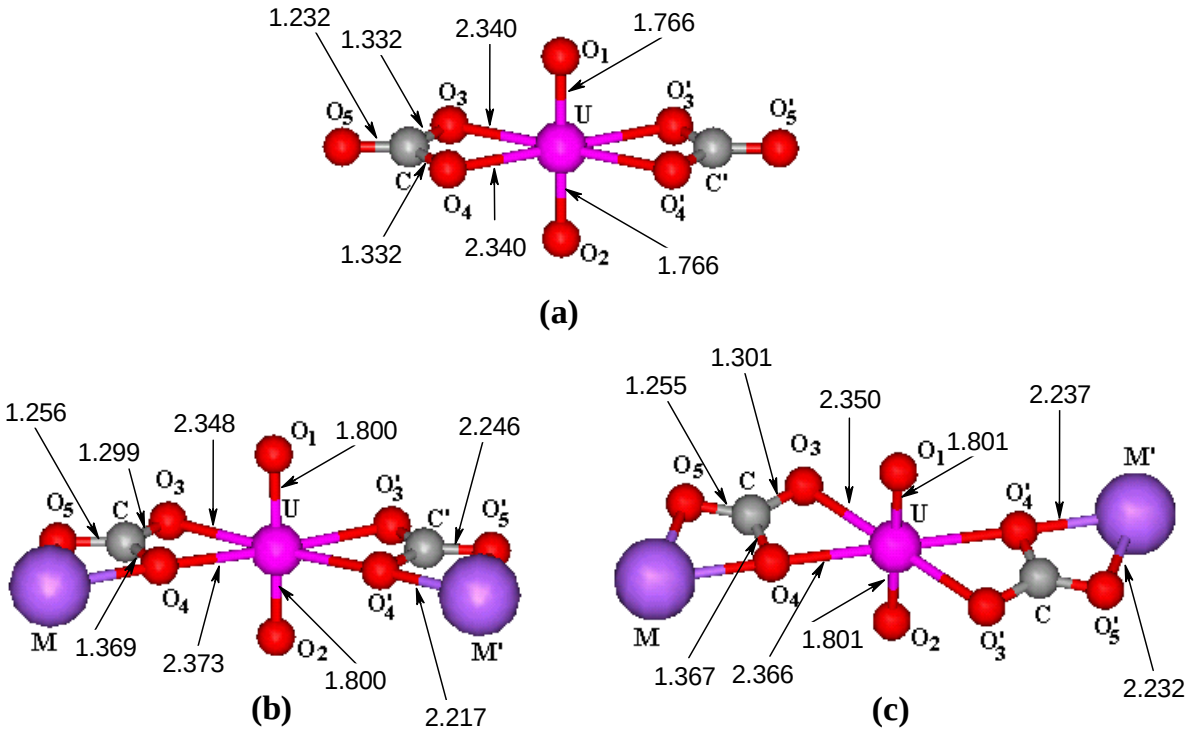

Fig 7 Computed Structures of $UO_2(CO_3)_2^{2-}$ and $UO_2(CO_3)_2M_2$.

concentration is relatively high and their stability in solution depends on the pH (pH=6). Our computed structures and spectra are shown in Figs 7 and 8, respectively. The IR spectra were obtained for the solid hydrated crystal of the compound $[C(NH_2)_3]_6[UO_2(CO_3)_6]$ and an unresolved shoulder for the O-U-O asymmetric stretch was observed at 915 cm^{-1}. This was masked by a strong carbonate out-of-plane deformation mode at 892 cm^{-1}. Using the relationship between the Raman active and IR active stretching modes, the O-U-O stretching mode was assigned as 911 cm^{-1} mode. More recently the IR spectra were obtained for the molecule $Ca_5[(UO_2(CO_3)_3]_2(NO_3)_2(H_2O)_{10}$. The absorptions at 1546, 1397, 740 and 690 cm^{-1} of this molecule were attributed to the carbonate group. The observed asymmetric stretch of UO_2^{+2} was at 900cm^{-1} one of the three weaker bands at 840, 825, and 816 cm^{-1} and was tentatively assigned to the symmetric-stretch modes. The O-U-O symmetric and asymmetric-stretch frequencies of $UO_2(CO_3)_2^{2-}$ are computed at 793 and 877 cm^{-1} in close agreement with the experiment. As seen from Fig 7, an unusual finding is that the $M_2UO_2(CO_3)_2$ (M = Li^+, and Na^+) complex has two structural arrangements viz., *cis*- (C_{2v}) and *trans*- (C_{2h}), the *trans*-isomer is only 1.25 kcal mol^{-1} more stable than the *cis*-isomer and thus both structures are probable in aqueous solution.

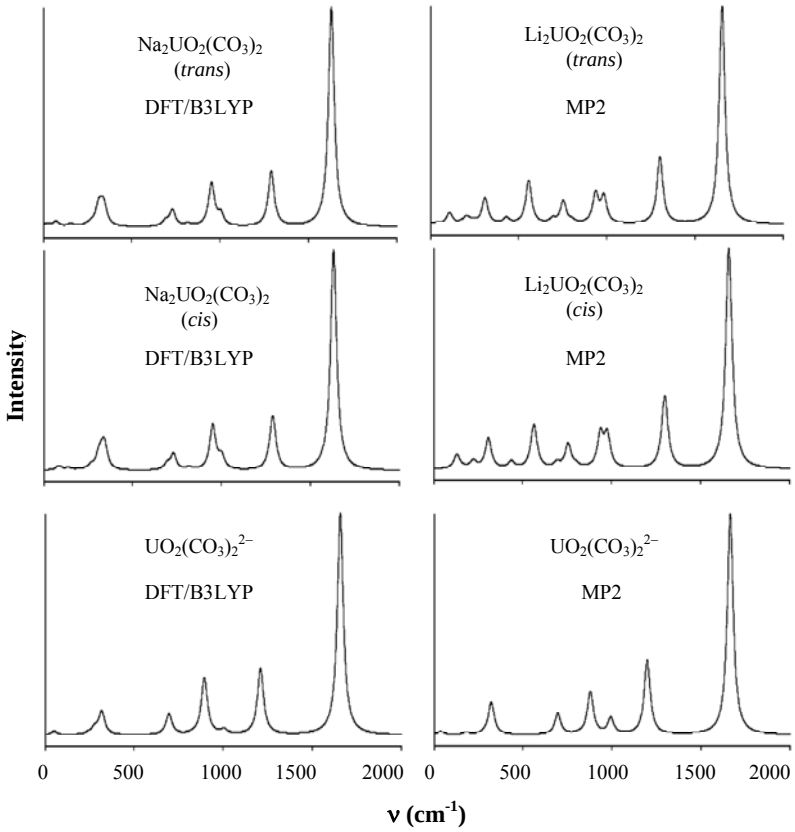

Fig 8 Computed IR spectra of $UO_2(CO_3)_2^{2-}$ and $UO_2(CO_3)_2M_2$.

5.2 Experiment Versus Theory: Uranyl Silicates and Arsenates

Our computational study was motivated by the experimental work of Prof. Nitsche and coworkers at Berkeley on U(VI) sorbed on silica gel which showed two different EXAFS spectra depending on the coverage or loading. Two structures shown in Fig 9 a & 9 B were proposed.

Fig.9a Atop complex of Uranium(VI) Sorbed on Silica Gel Interface (load 0.5 mg U/g)

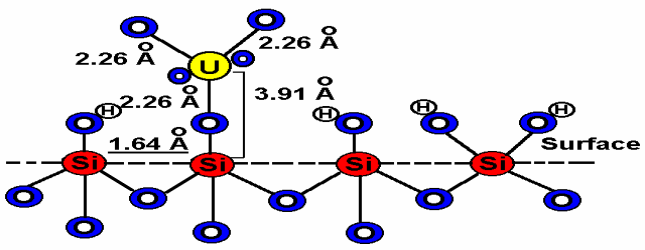

Fig. 9b Two Bridged Structures for U(VI) sorbed on Silica Gel (load 5 - 70 mg U/g)

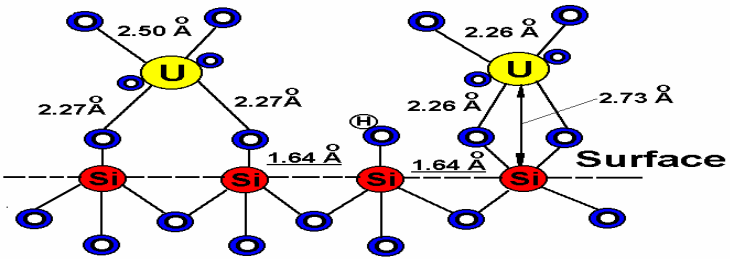

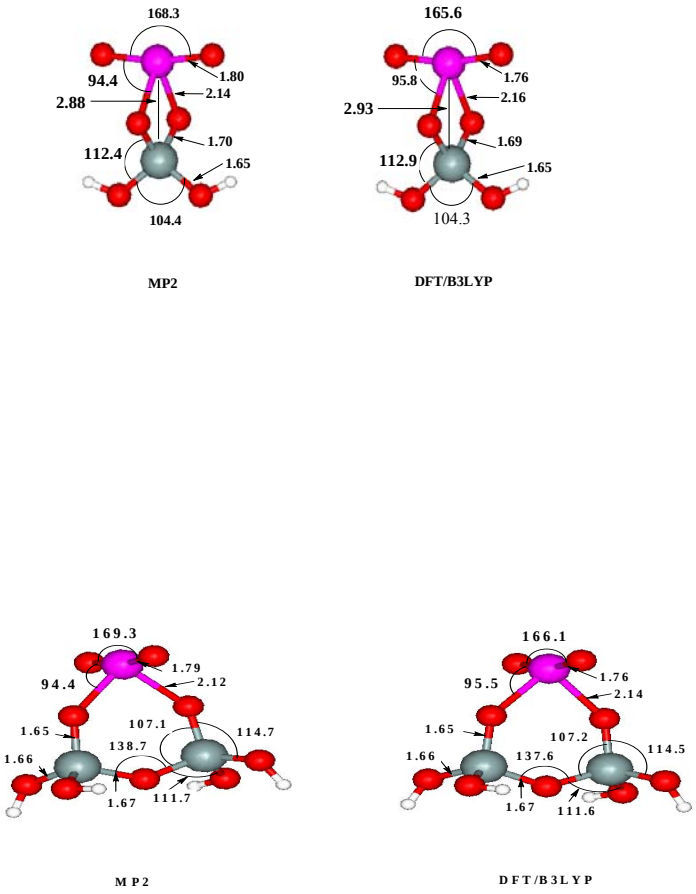

Fig 10 Two different computed structures for uranyl silicates confirming experiment.

Our computations results on model uranyl silicate complexes shown in Fig 10 indeed confirmed the existence of two possible optimized potential minima, one called a-top and the other bridge structure.

We have carried out extensive *ab initio* calculations on the structure and spectra of $H_2UO_2SiO_4.3H_2O$, $HUO_2PO_4.3H_2O$, and $HUO_2AsO_4.3H_2O$. The calculated structures and vibrational spectra have been compared with the available experimental data. The silicate, phosphate and arsenate minerals are quite abundant in nature and their structural and bonding studies are important to the understanding of the mobility of uranium in natural systems and in soils contaminated by actinides. The USi3W molecule has been studied very recently in solid form through EXAFS technique. The phosphate and the arsenate molecules are studied as the simplest forms of the corresponding uranyl compounds $(UO_2)_3(PO_4)_2(H_2O)_4$, and

$(UO_2)[(UO_2)(AsO_4)]_2(H_2O)_4$. The geometry optimization of USi3W, UP3W, and UAs3W at both the DFT/B3LYP and MP2 levels show that the water molecules in these tri-hydrated complexes lie in a plane containing the uranium and the silicate, phosphate or arsenate group, and thus forming pentagonal bi-pyramid structures. We have compared the calculated geometries with the available crystal structure data and the agreement is quite satisfactory at both the DFT/B3LYP and MP2 levels. Our calculated vibrational spectra of USi3W compare quite well with the observed vibrational spectra of $(UO_2)_2SiO_4.2H_2O$. We have compared the calculated $U\text{-}O_3$ and $U\text{-}O_4$ distances of these molecules. They show that the uranyl-silicate and uranyl-phosphate interactions would be similar and the uranyl-arsenate interaction would be less than both of them.

5.3 Aqueous Complexes of $UO_2^{2+}(H_2O)_n$, $NpO_2^{+}(H_2O)_n$,, and $PuO_2^{2+}(H_2O)_n$ [20,26]

The hydrolysis reactions of urnayl, neputyl and plutonyl complexes have received considerable attention due to their geochemical and biochemical importance but the results of free energies in solution and the mechanism of deprotanation have been topic of considerable uncertainty. We have computed deprotonating and migration of one water molecule from the first solvation shell to the second shell in $UO_2(H_2O)_5^{2+}$, $NpO_2(H_2O)_6^{+}$, and $PuO_2(H_2O)_5^{2+}$ complexes.[20,26] Our computed Gibbs free energy(7.27 kcal/m) in solution for the first time agrees with the experiment (7.1 kcal/m) while previous computations produced results in strong disagreement. We concluded that for $UO_2(H_2O)_6^{2+}$, the binding energies of the sixth water in the first shell or the second shell are quite close and thus six-coordination might occur in solution. Our computed solvation free energies also suggest that five- and six-coordination are equally preferred for UO_2^{2+}, whereas only five-coordinated species are preferred for NpO_2^{+} and PuO_2^{2+}. The gas-phase vibrational frequencies show interesting features as a function of the hydration coordination and the computed asymmetric axial U-O stretches agree quite well with experiment. The gas phase vibrational frequency computations were very intensive at the CCSD level as this had to be done at the numerical level. Overall the frequency trends at the CCSD level confirm the MP2 results. We have also shown that the computed vibrational spectra (fig. 11) and structures in solution differ (see Fig 12) enough to warrant reoptimization of the structures in solution.

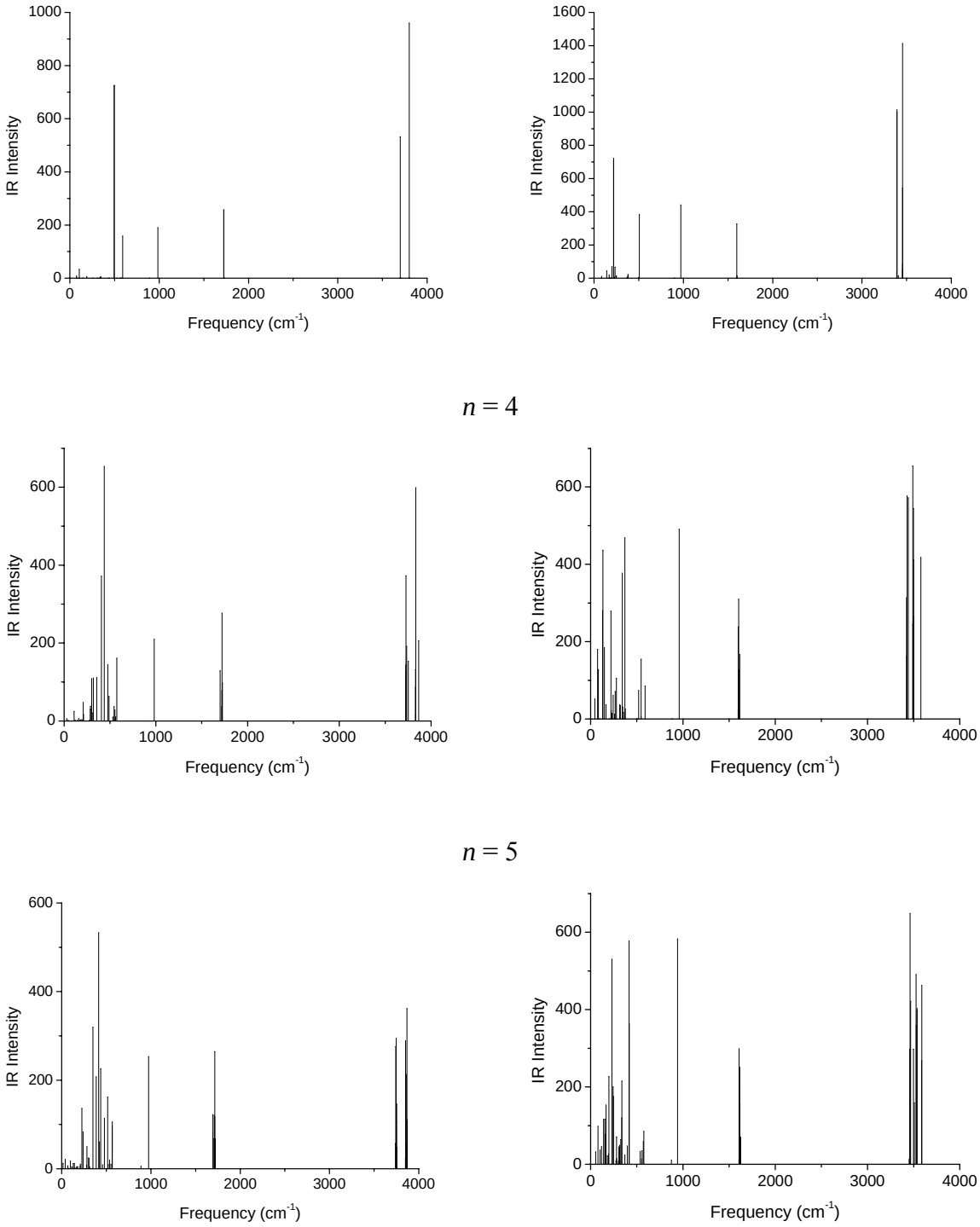

Fig 11 Computed IR spectra of $UO_2(H_2O)_n^{2+}$ in gas phase and aqueous solution.

We have also considered the reaction $AcO_2(H_2O)_5^{2+} + H_2O \rightarrow AcO_2(H_2O)_4(OH)^{2'+} + H_3O^+$, quite important in bio and geo environments. Fig 12 shows substantially different structures s in the gas phase and solution for $NpO_2(H_2O)_4OH$.. For the first time such a substantially differing structures have been found in gas phase versus solution.

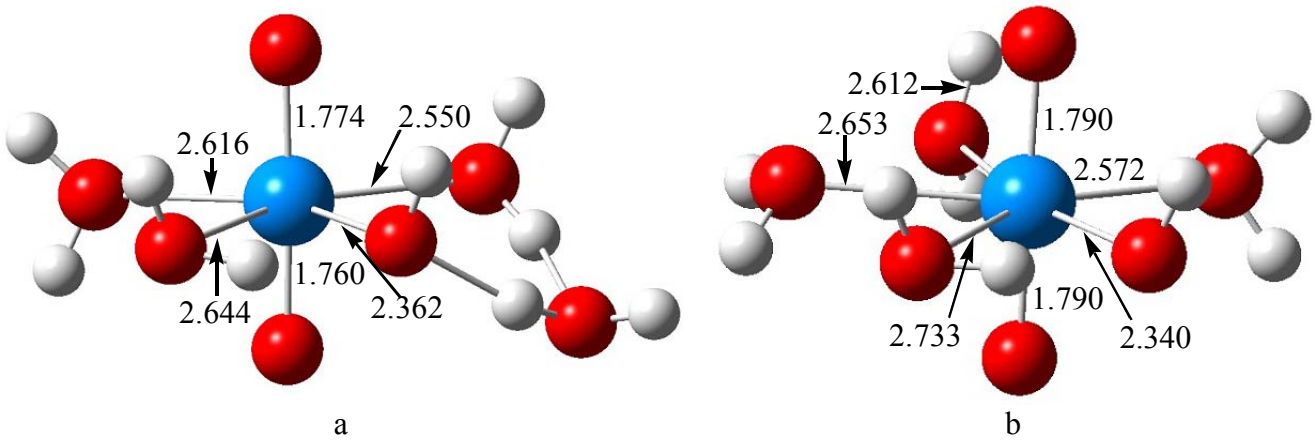

Fig. 12. Optimized $NpO_2(H_2O)_4(OH)$ in the gas phase (a) and aqueous solution (b).

5.4 Fluxional Motions and Internal Rotations in Actinyl complexes.[24]

We have computed the torsional tunneling barriers for water molecules bound to actinyl ions, UO_2^{2+}, NpO_2^+, and PuO_2^{2+} using high-level relativistic computations in aqueous solution. We show that the barriers drop substantially as a function of number of water molecules, resulting fascicle exchange of water molecules from the solvent to the complex**.**

Clark et al. at Los Alamos National Lab have shown that the uranyl ions under alkaline conditions exhibited oxoligand exchange with the solvent using ^{17}O variable temperature width NMR. They have established that the ^{17}O NMR spectra behavior is consistent with a ligand exchange process that is slow on the NMR time scale. A remarkable finding by Clark et al. is that the ^{17}O NMR spectra of the uranyl species in solution showed either no oxoresonance or only a weak signal due to U and O. This suggests non-rigid chemical exchange between the complex and solvent H_2O molecules.

We computed the barriers to internal rotations of water molecules bound to actinyl ions in solution. Fig 13 shows our computed structures while Fig 14 shows the computed barriers for the internal rotation as a function of number of water molecules. As can be seen from Fig. 14, when the first hydration shell is completed at n=5, the barrier for internal rotation substantially reduces to such a small value of (0.2 kcal/m) that there is fascicle exchange of solvent H_2O molecules with the fifth molecule weakly bound in the fist hydration shell, thus explaining the observed spectra. Fluxional motions in actinyl complexes are truly exciting.

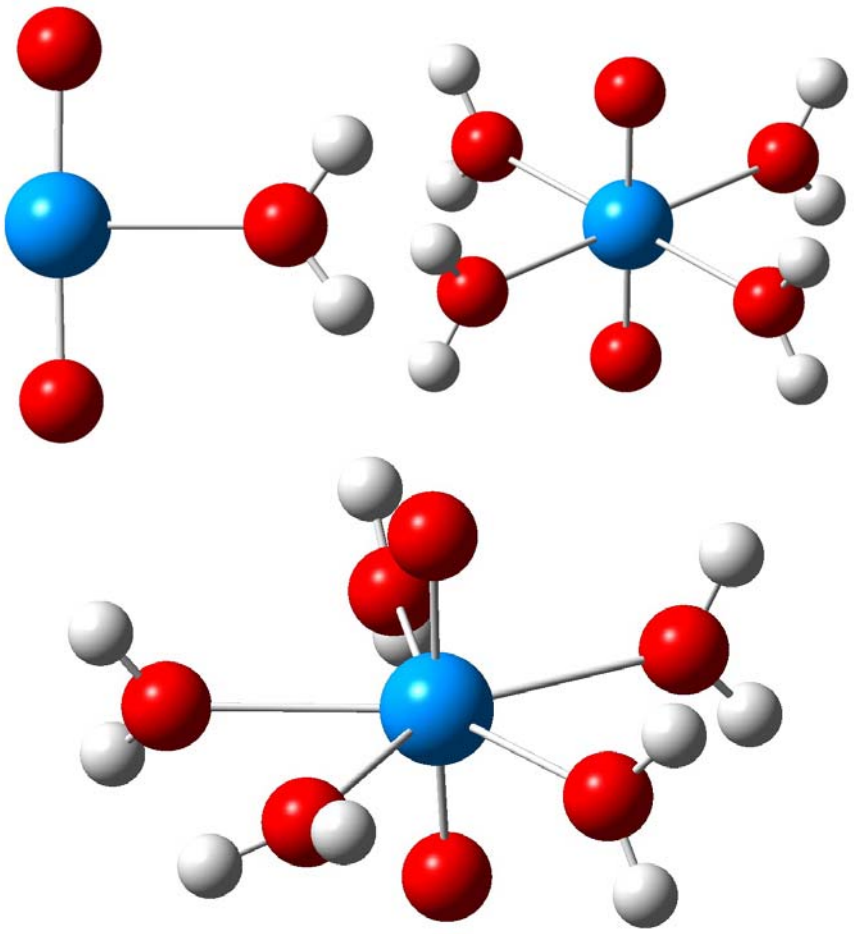

Fig 13 Computed Structures of $AcO_2(H_2O_n)^{2+}$

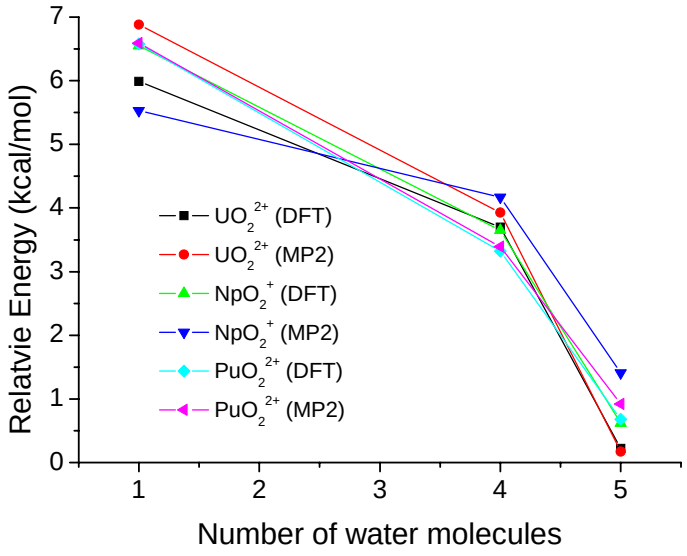

Fig 14 Internal Rotation barriers for water molecules as a function of n.

5.5 Plutonyl Silicates and Carbonates[15,23,27]

We have studied the electronic and spectroscopic properties of plutonyl carbonate complexes of the types PuO_2CO_3 and the hydrated forms, $PuO_2CO_3.nH_2O$, (n=1,2).[15] Our computed equilibrium geometries and vibrational spectra of these species agree quite well with the EXAFS and Raman data available on related complexes. We have reported the results of ab initio quantum chemical computations on the plutonyl carbonate complex and its hydrated forms, viz., PuO_2CO_3, $PuO_2CO_3.H_2O$ and $PuO_2CO_3.2H_2O$. The results of our computations at the DFT, MP2 and CCSD levels show that the computed geometries and vibrational frequencies are in reasonable agreement among these theoretical levels. Our computed geometries for the various interatomic distances at both MP2 and DFT levels agree quite well with the experimental EXAFS results of Clark et al. at Los Alamos in solution for the limiting $Pu(VI)O_2$-carbonate complex. Our predicted equatorial carbonate vibrational mode frequency of 754 cm^{-1} at the MP2 level is consistent with the observed Raman band at 755 cm^{-1} in solution form of plutonyl carbonate complex.

We have also studied the properties of plutonyl carbonate complexes of the types $PuO_2(CO_3)_3Ca_3$[23], which are extremely important from experimental standpoint, as these species have been observed in aqueous solution. The plutonyl silicates are extremely interesting as these complexes play a vital role in the transport of pultonyl ions bound to colloidal silicates as shown by Dr. Annie Kersting at Lawrence Livermore National Lab. Thus we have studied the bonding and complexation of plutonyl with silicates[27] which for the first time provided interpretation of how plutonyl ions bind to colloidal silicates and transport in the aquatic environment.

6. Developments, Code Enhancements, etc.

We have been constantly striving to improve the codes and ensure the techniques are accurate and state of the art. For example, in a recent work, we have calibrated the accuracy of RECPs (relativistic effective core potentials) using all-electron relativistic Douglas-Kroll method. We have found that the bond distances computed using RECPS came within 0.005-0.01 A depending on the electronic state. The energy separations were also quite accurate except that the DK method does not include spin-orbit coupling and thus the RCI results were more accurate when spin-orbit effects were included.

Significant code developments, code modernization and porting of codes to multiple computational platforms and significant enhancement of the RCI codes were accomplished. Originally ALCHEMY II set of codes were designed for primarily IBM-based platforms such as

IBM RS/6000. Dr. Megu Yoshimine started porting the non-relativistic part of the codes to other platforms such as Windows 'XP based systems. Encouraged by these developments, we continued the porting and major enhancements so that we can carry out multi-reference relativistic computations that include up to 60 million configurations in Windows XP and linux workstations. The major bottleneck to such enhancements were (1) multiple entry points in subroutines that created variable definition problems in other compilers (2) current limitations in direct access data files of 2^{30} bytes or less than 2 GB/file (3) limitations of sequential data files to 4 GB/file, etc. We have surmounted all of these barriers by significant revamping of the symbolic CI integral sort, and direct CI diagonalization codes. The symbolic CI technique, which constructs the needed formulas, uses two direct access files that grow in size rapidly as the number of symbolic CSFs increase. Even with the multiple pass algorithm the need space exceeds the limit of 2 GB for direct access files and sequential files that store the off-diagonal symbolic matrix elements also grow in size. We modified the codes to split into multiple direct access files, each within 2 GB limit so that we can carry out large-scale CI computations up to 35 million at present. Likewise the off-diagonal sequential access file had to be split into several files as it exceeds 4 GB limit, but this lead to many modifications in numerous places in the both symbolic sort and direct CI diagonalization.

The other major development had to do with the RCI code enhancements. The RCI codes were enhanced and interfaced with ALCHEMY 2002 codes so that large CIs and multiple roots can be done. The current version of the code routinely extracts 100 RCI states per CI diagonalization and up 100,000 reference configurations.

Both ALCHEMY 2002 codes and the RCI codes have been ported to the Windows XP, linux platforms and they also run on IBM RS/6000 platforms. We are thus poised to carry out large-scale relativistic computations containing both large number of configurations and basis sets.

7. References & Publications of DOE-Award DE-FG02-04ER15546

1. R. Guo and K. Balasubramanian, "Theoretical study of the low-lying electronic states of ruthenium trimer (Ru_3)", *J. Chem. Phys.* **118**, 142-148 (2003)

2. S. Roszak and K. Balasubramanian, **"**Electronic structure and spectroscopic properties of electronic states of VC_2, VC_2^-, and VC_2^+", *J. Chem. Phys.* **118** 130-141 (2003).

3. D. Majumdar, S. Roszak K. Balasubramanian, and H. Nitsche" Theoretical study of aqueous uranyl carbonate (UO_2CO_3) and its hydrated complexes: $UO_2CO_3.nH_2O$ (n = 1 - 3)", *Chemical Physics Letters* **372**, 231-238 (2003).

4. V. Wheaton, D. Majumdar, K. Balasubramanian, L. Chauffe, and P. G. Allen, "A Comparative Theoretical Study of Uranyl Silicate Complexes", *Chemical Physics Letters* **371**, 349-356 (2003).

5. D. Majumdar and K. Balasubramanian, "A theoretical Study of Potential Energy Curves and Specroscopic Constants of VC", *Molecular Physics* **101**, 1369-1376 (2003).

6. R. Guo, K. Balasubramanian and H. F. Schaefer III, "The Treacherous Potential Energy hypersurface of AgSiO", *J. Chem. Phys.* **118**, 10623-10630(2003).

7. K. Balasubramanian, W. Siekhaus and W. McLean II, "Potential Energy Surfaces for the Uranium Hydridng and UH_3 Catalysis", *J. Chem. Phys.* **119**, 5879-5900(2003).

8. D. Majumdar and K. Balasubramanian, "Theoretical study of the electronic states of Niobium Trimer (Nb_3) and its anion (Nb_3^-)", *J. Chem. Phys.* **119**, 12866-12877 (2003).

9. R. Guo and K. Balasubramanian, "Spectroscopic Constants and Potential Energy Curves of Ruthenium Carbide: RuC", *J. Chem. Phys.* **120**, 7418-7425(2004).

10. Lester Andrews, Xuefeng Wang, and K. Balasubramanian, "The Gold Dihydride Molecule, AuH_2: Calculations of Structure, Stability and Frequencies, and the Infrared Spectrum in Solid Hydrogen", *J. Phys. Chem A*. **108**, 2936-2940 (2004).

11. K. Balasubramanian, "Relativity and the Periodic Table", (D. Rouvary & R. B. King, editors), Periodic Table into the 21st Century, 2004

12. K. Balasubramanian, "Relativistic Double Group Spinor Representations of Non-rigid Molecules", *J. Chem. Phys.* **120**, 5524-5535(2004).

13. D. Majumdar and K. Balasubramanian, "Theoretical Study of the Electronic States of Nb_4, Nb_5 clusters and their anions (Nb_4^-, Nb_5^-), *J. Chem. Phys.* **121,** 4014-4032 (2004).

14. K. Balasubramanian, "Mathematical Basis of Periodicity in Atomic and Molecular Spectrsocopy", Mathematics of the Periodic Table, Editors: R. B. King and D. H. Rouvray, Nova Press, NJ 2004

15. D. Chaudhuri and K. Balasubramanian, "Electronic Structure and Spectra of Plutonyl Complexes and their hydrated forms: PuO_2CO_3 and $PuO_2CO_3.nH2O$ (n=1,2)", *Chemical Physics Letters*, 399, 67-72 (2004)

16. D. Majumdar and K. Balasubramanian, "Theoretical studies on uranyl–silicate, uranyl–phosphate and uranyl–arsenate interactions in the model $H_2UO_2SiO4 \cdot 3H_2O$, $HUO_2PO_4 \cdot 3H_2O$, and $HUO_2AsO_4 \cdot 3H_2O$ molecules", *Chemical Physics Letters,* **397**, 26-33 (2004).

17. D. Majumdar and K. Balasubramanian, "Theoretical studies on the electronic structures of $UO_2(CO_3)_2^{2-}$ and its metal salts: $M_2UO_2(CO_3)_2$ (M = Li^+, and Na^+)", *Molecular Physics,* **103**, 931 – 938(2005)

18. P. A. Denis and K. Balasubramanian, "Spectroscopic Constants and Potential Energy Curves of low-lying electronic states of NbC", J. Chem. Phys. **123**, 054318 (2005) –Published online 9Aug 2005.

19. K. Balasubramanian, "Relativistic Effects in the Chemistry of very Heavy and super heavy Molecules", Lecture Series on Computer & Chemical sci. 4, 759-764 (2005) UCRL-JC-145416

20. Z. Cao and K. Balasubramanian, "Theoretical Studies of hydrated complexes of uranyl, neptunyl and plutonyl in aqueous solution: $UO_2^{2+}(H_2O)_n$, $NpO_2^{2+}(H_2O)_n$, and $PuO_2^{2+}(H_2O)_n$", J. Chem. Phys. **123**, 114309-1 to 114309-12 (2005)

21. P. A. Denis and K. Balasubramanian, "Spectroscopic Constants and Potential Energy Curves of low-lying electronic states of MoC", J. Chem. Phys. 125, 024306-1, 024306-9 (2006)

22. P. A. Denis and K. Balasubramanian, "Spectroscopic Constants and Potential Energy Curves of low-lying electronic states of ZrC", J. Chem. Phys. **124**, 174312 (2006).

23. D. Chaudhuri and K. Balasubramanian, "Electronic Structure and Spectra of di and tri carbonate complexes of Plutonyl: $PuO_2[CO_3]_2$ and $PuO_2[CO_3]_3Ca_3$ ", *Chemical Physics Letters*, to be submitted

24. K. Balasubramanian and Z. Cao, "Fluxional Motions and internal rotational barriers of Water molecules bound to UO_2^{2+}, NpO_2^{+}, and PuO_2^{2+}", Chemical Physics Letters , submitted

25. B. Suo and K. Balasubramanian, "Spectroscopic Constants and Potential Energy Curves of Yttrium Carbide: YC", J. Chem. Phys., submitted.

26. Z. Cao and K. Balasubramanian, "Proton transfers and Hydration Energies of solvated actinyl ions in aqueous solution: Unusual structures", J. Chem. Phys. To be submitted

27. D. Chaudhuri and K. Balasubramanain, "Geometrical and Electronic Structures of Plutonyl Silicates", in preparation